Chiral Polymers Hot Paper

How to cite: *Angew. Chem. Int. Ed.* **2022,** *61,* e202115070
International Edition: doi.org/10.1002/anie.202115070
German Edition: doi.org/10.1002/ange.202115070

Dissymmetric Chiral Poly(diphenylacetylene)s: Secondary Structure Elucidation and Dynamic Luminescence

*Juan José Tarrío, Rafael Rodríguez, Berta Fernández, Emilio Quiñoá, and Félix Freire**

Abstract: The secondary structure of a dissymmetric and chiral poly(diphenylacetylene) (PDPA) is elucidated by combining the data from NMR experiments (regioregular head to tail structure), Raman and IR studies (*E* configuration of the polyene double bonds), and high-resolution AFM images (helical pitch, packing angle and orientation of the external helix). As a result, an *E-transoidal* polyene backbone describing three coaxial helices is obtained. Theoretical electronic circular dichroism (ECD) studies of the structure show a good correspondence between experimental and theoretical data and allow one to decipher that the first Cotton band is generated by the poly(diphenylacetylene) core and not only by the polyene backbone. The dynamic behavior of poly-(*S*)-**2** is also demonstrated by a helix inversion effect produced by conformational changes at the pendant groups when annealed in solvents with different donor abilities. This phenomenon is accompanied by an inversion of the circular polarized luminescence of the PDPA (CPL switch).

Introduction

Molecular engineering allows the design of novel materials with a certain structure and specific properties related to it. Within this topic, modelling new helical structures based on non-natural building blocks such as helicenes,[1–3] foldamers,[3–6] supramolecular[7–9] or covalent helical polymers,[10–17] has attracted the attention of the scientific community. These studies are inspired by the structure/function relationships present in biomacromolecules such as peptides, proteins, DNA or polysaccharides. Among non-natural helical scaffolds, dynamic helical polymers constitute a very interesting family due to the possibility of tuning their helical sense or elongation through external stimuli.[19–23] The use of non-natural building blocks to synthetize these polymers allows the creation of smart materials with applications in different fields such as sensing,[24–31] asymmetric synthesis,[32–36] chiral recognition[37] and separation.[38–41] However, in molecular engineering it is mandatory to establish structure/function relationships for these materials, a fact that will allow to determine and, if possible, refine the structural features involved in the functionality of the material.

Unfortunately, the structural elucidation of helical polymers is not straightforward due to the presence of monomer repeating units (m.r.u.) along the polymer chain, rendering powerful structural techniques such as nuclear magnetic resonance (NMR) or X-ray diffraction (XRD) useless. During the last decade a great effort has been made in the structural characterization of poly(phenylacetylene)s (PPAs), fundamentally through a combination of techniques (NMR,[42,43] XRD,[44–52] atomic force microscopy (AFM),[53–61] differential scanning calorimetry (DSC),[62] Raman,[63] circular dichroism (CD),[64,65] vibrational circular dichroism (VCD),[66] Raman optical activity (ROA),[67]), computational studies[68,69] and reactivity experiments (photochemical electrocyclization of PPAs[67]) that were used to obtain information about different structural parameters of these complex macromolecules and combined to solve the puzzle of the secondary structure of helical polymers.

Another interesting family of helical polymers are the poly(diphenylacetylene)s (PDPAs)[71–93] that resemble PPAs in the main chain, which in both cases is made up of conjugated double bonds. However, the presence of a phenyl group on each carbon of the double bond in PDPAs makes the properties of both materials very different. For instance, PDPAs show better chemical, thermal and photochemical stability compared to PPAs.[72–85] Moreover, PDPAs exhibit another interesting property that PPAs do not have, i.e. photoluminescence.[82–85,89] As a negative characteristic, PDPAs show a poor dynamic behavior, being necessary to heat them to 80° to induce a helical sense once the external stimuli are modified.[79–85] This depletion of dynamic behavior is a consequence of the introduction of the second phenyl ring in the m.r.u., which congests the

[*] J. J. Tarrío, Prof. E. Quiñoá, Prof. F. Freire
Centro Singular de Investigación en Química Biolóxica e Materiais Moleculares (CiQUS) and Departamento de Química Orgánica
Universidade de Santiago de Compostela
15782 Santiago de Compostela (Spain)
E-mail: felix.freire@usc.es

Dr. R. Rodríguez
WPI Nano Life Science Institute (WPI-NanoLSI)
Kanazawa University
Kakuma-machi, Kanazawa 920-1192 (Japan)

Prof. B. Fernández
Departamento de Química Física
Universidade de Santiago de Compostela
15782 Santiago de Compostela (Spain)

helical backbone and where steric repulsion does not favor chiral amplification and helix inversion effects.

PDPAs can be classified in two different groups, symmetric (Scheme 1a) or asymmetric (Scheme 1b), depending on the substitution of the two phenyl rings. Moreover, in both groups the stereoregularity of the polymer depends on the configuration of the double bonds, *Z* or *E* (Scheme 1a, b), and the dihedral angle between conjugated double bonds, which can adopt either cisoidal or transoidal configuration, $\omega_1 < 90°$ (cisoidal); $\omega_1 > 90°$ (transoidal) (Scheme 1c). Thus, four different possible stereoregularities can be obtained in PDPAs, namely *Z-cisoidal, Z-transoidal, E-cisoidal and E-transoidal*, where the *Z*/*E* content depends on the catalyst used for the polymerization reaction and the cisoidal/transoidal configuration is related to the steric hindrance between pendant groups.

The complexity of the system increases in the case of asymmetric PDPAs where different products can be obtained depending on the regioregularity of the polymerization reaction. Thus, head-to-tail, head-to-head or tail-to-tail polymerizations can occur (Scheme 1d), each of them with the four possible stereoregularities at the conjugated polyene backbone.

This fact, in combination with the fully substitution of the double bonds, and therefore of the polyene backbone, makes the extrapolation of structural information obtained for PPAs useless to elucidate the structure of PDPAs.

Only a few examples related to chiral PDPAs[72–85] are found in the literature compared to the large amount of work that has been done with PPAs.[12–33,37–51,94–97] This is due to the difficulty of obtaining the former polymers in the laboratory by polymerization of the corresponding diphenylacetylene monomers (DPA). Thus, while PPAs bearing a large variety of functional groups are easily prepared using a Rh^I catalyst,[45,51] the synthesis of PDPAs is more complex due to the low tolerability towards polar groups shown by the catalysts used to prepare these materials. For instance, Tang and co-workers developed a synthetic procedure that uses a combination of WCl_6-Ph_4Sn in toluene to polymerize achiral diphenylacetylenes,[74–76] although following this approach it is not possible to polymerize diphenylacetylenes bearing polar groups due to the poisoning of the catalyst. To prepare polar PDPAs, it is neccessary to first polymerize a diphenylacetylene in which one or both of the aryl rings carry an active pentafluorophenyl ester group (PFP), which is efficiently transformed into a chiral PDPA by a post-functionalization reaction.[81] Interestingly, all the polymers prepared in these conditions do not show an induced helical structure once they are obtained. Thermal annealing is necessary, i.e., 4 h at 80 °C, to induce a preferred handedness in the PDPA main chain.[81,82,86,99]

Recently, Maeda and co-workers studied the secondary structure of symmetric PDPAs bearing para-substituted carboxy pendant groups.[79,80] By using a combination of ^1H and ^{13}C NMR, IR, Raman, VCD and ECD spectroscopies, they found that this polymer adopts a preferred *cis-transoidal* structure, where *P* or *M*-helical senses can be induced by thermal annealing in water in the presence of chiral amines. On the other hand, in the case of asymmetric PDPAs, Kwak, Aoki and co-workers made great contributions to the study of their luminescent properties and to the achiral-to-chiral transformations of PDPAs.[78,82,85–89] To perform these studies, a catalyst developed by Masuda [$TaCl_5$-n-Bu_4Sn] was used.[77] Also with asymmetric PDPAs, Tang and co-workers reported polymers prepared with the WCl_6-Ph_4Sn[83,84] catalyst that Maeda also employed for the preparation of optically active PDPAs with application as chiral stationary phases.[71] Nevertheless, although several examples of asymmetric PDPAs are found in literature, their secondary structure remains unclear. From these studies it is found that the helical structure adopted by a PDPA depends on the monomer structure[98] and, therefore, to assume that symmetric and asymmetric PDPAs have the same scaffold is a mistake.

Herein, we will study the secondary structure of chiral and asymmetric PDPAs obtained from polymerization of an achiral diphenylacetylene, where one of the aryl rings carries an active pentafluorophenyl ester (PFP) group, while the other phenyl ring remains unaltered.[81] This approach is one the most widely used in the preparation of asymmetric PDPAs. The stereo and regioregularity of the polymer will depend on the synthesis of the first PDPA, which bears the PFP as pendant group and that is further transformed in a chiral PDPA. Thus, through a post-functionalization reaction, the PDPA bearing the 4-benzamide of alanine methyl ester as pendant group will be prepared and its secondary structure elucidated.

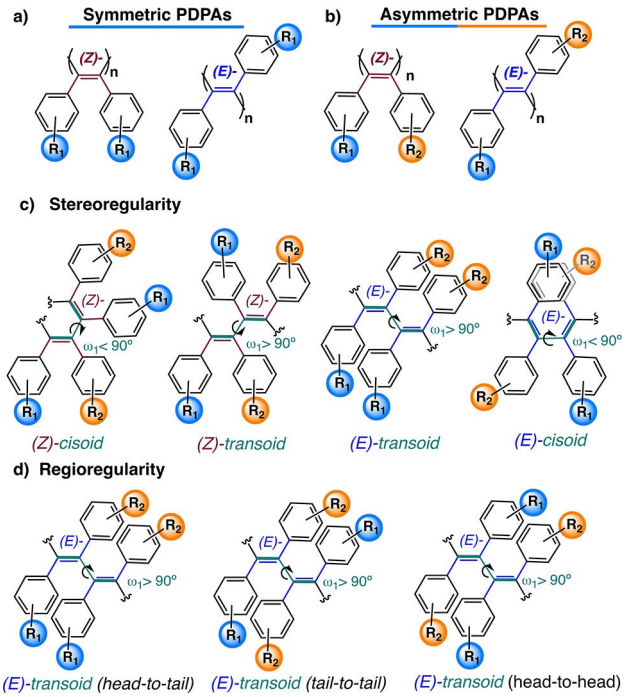

Scheme 1. General molecular structure of a) symmetric and b) asymmetric PDPAs. c) Stereoregularity of a PDPA obtained via head to tail polymerization. d) Regioregularity in a PDPA with an (*E*)-transoidal polyene backbone.

Results and Discussion

The synthesis of the achiral and asymmetric precursor, perfluorophenyl 4-(phenylethynyl)benzoate, and its subsequent polymerization to obtain poly-**1** using a mixture of WCl_6-Ph_4Sn as catalyst, was carried out according to the methods previously reported.[83,84]

The number average molar mass (M_n) and molar mass dispersity (M_w/M_n) of poly-**1** were 1.4×10^4 and 1.43 respectively, as determined by gel permeation chromatography (GPC) using THF as eluent and polystyrene narrow standards (PSS) as calibrants. Taking advantage of the active ester present as pendant group, poly-**1** was effectively transformed into poly-(*S*)-**2** by coupling with NH_2-Ala-OMe under common peptide coupling conditions (Figure 1), as confirmed by ^{19}F NMR and IR studies that corroborated the disappearance of the signals corresponding to the pentafluorophenol moeity (see Supporting Information).

Once poly-**1** and poly-(*S*)-**2** were obtained, their stereo- and regioregularity were analyzed using IR, Raman, and NMR techniques as structural tools.

Raman spectroscopy is a powerful structural technique that provides useful information related to the stereoregularity of the conjugated double bonds.[83] It is commonly applied to assess *cis*- or *trans*-content in PPAs and PDPAs.[51,99,100] Catalysts based on tungsten (W) are known to provide *trans*-rich PDPAs as shown in many examples in the literature,[99,100] albeit Maeda recently demonstrated that in the case of symmetric PDPAs, polyene backbones with a predominant *cis*-content of double bonds are also obtained.[79,80]

Herein, we will study the stereoregularity of poly-**1** and poly-(*S*)-**2** by comparison of their Raman spectra with those obtained for PPAs with well-known secondary structure. Therefore, as model compounds we chose poly-(**3**–**6**) (Figure 2a). Poly-**3**[100] and poly-**4**[54] were selected due to their resemblance with poly-**1** and poly-(*S*)-**2**, while poly-**5**[70] and poly-**6** were chosen due to the possibility of generating a *trans*-PPA (*E*-PPA, poly-**6**) by isomerization of a *cis*-PPA (*Z*-PPA, poly-**5**) (Figure 2a). The isomerization of the polyene backbone proceeds through the generation of a delocalized radical cation in the polyene when the anilide group of the PPA interacts with Au^{3+} (see Supporting Information).

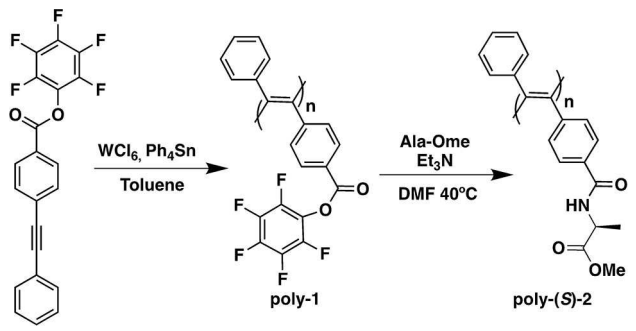

Figure 1. Synthetic approach to prepare poly-**1** and poly-(S)-**2**.

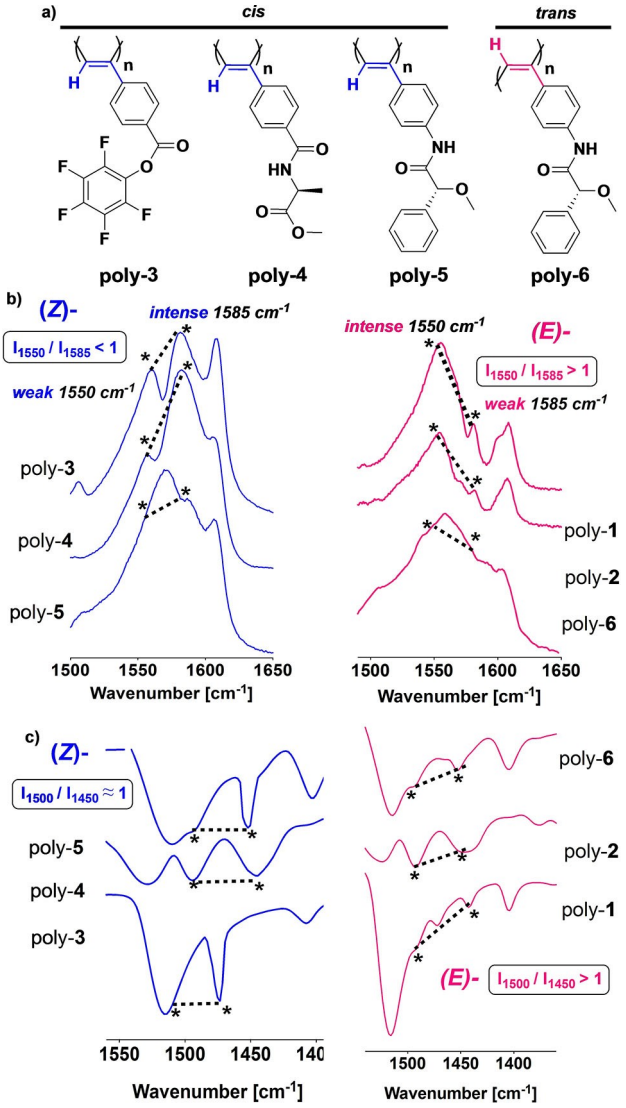

Figure 2. a) Structure of poly-(**3**–**6**). Partial b) Raman and c) IR spectra of poly-(**1**–**6**) showing the 1300–1600 cm^{-1} regions.

Careful examination of the Raman spectra unambiguously reveals clear differences for the polymeric backbones containing *cis* or *trans* double bonds. While polymers with a high content of *cis* (*Z*) double bonds [poly-(**3**–**5**)] showed an intense Raman band at ca. 1585 nm together with a weak one at ca. 1550 nm, for polymers with a *trans* (*E*) configuration [poly-(**1**–**2**), poly-**6**] of the double bonds, the opposite scenario is obtained, a weak band at ca. 1585 nm followed by a strong band at ca. 1557 nm (Figure 2b).

Another structural technique that provides useful information related to the *Z*/*E* configuration of double bonds in polyene backbones is IR. In a seminal work, Simionescu et al. were able to determine the *cis*/*trans* (*Z*/*E*) configuration of the double bonds by analyzing the ratio between the bands at 1500 and 1450 cm^{-1} of different model compounds.[101] Thus, while PPAs with a 1500/1450 (cm^{-1}/cm^{-1}) ratio > 1 have a majority *trans* configuration of the double bonds, those with a 1500/1450 (cm^{-1}/cm^{-1}) ratio ≈ 1

have a prevalent *cis* configuration of the double bonds. Hence, we decided to analyze these bands for all the polymers used in this study, PPAs and PDPAs, and determine if the reported pattern found by Simionescu et al. for PPAs can be extended to PDPAs. Interestingly, in all PDPAs and PPAs with a *trans*- (*E*) content of the double bonds, the ratio between the 1500/1450 (cm^{-1}/cm^{-1}) bands is greater than 1, while in those cases where the polyene is formed by *cis*- (*Z*) double bonds, the ratio between those two bands is ≈1, indicating that this PPA protocol can be extended to PDPAs (Figure 2c).

To determine the *Z*/*E* configuration of the double bonds, it is recommended to analyze both the Raman and IR spectra, being necessary to check the ratio of signals at ca.1585/1550 (cm^{-1}/cm^{-1}) for Raman studies and ca.1500/1450 (cm^{-1}/cm^{-1}) for IR experiments.

Once the *trans* (*E*) configuration of the double bonds was demonstrated in asymmetric PDPAs prepared with WCl_6/Ph_4Sn catalysis, the regioregularity of these polymers was explored.

As stated above, different regioregularities (head-to-tail, head-to-head, and tail-to-tail) can be generated in these systems during the polymerization of asymmetric DPA monomers (Scheme 1d). ^{1}H NMR spectra of poly-(*S*)-**2** in different solvents show a single set of NMR signals indicating the presence of a regioregular polymer (Figure 3c and Supporting Information). Otherwise, a mixture of regioregularities should result in more complicated NMR spectra due to the different anisotropic environments experienced by the protons of the m.r.u. within the different regiochemistries (Figure 3a). To discriminate between the different regioregularities, long-distance 2D NMR experiments such as NOESY were carried out. Detailed observation, after modeling structures containing the three possible regioregularities (head-to-tail, head-to-head, and tail-to-tail) of poly-(*S*)-**2** and *trans* (*E*) configuration of the double bonds in the polyene backbone, reveals that in head-to-head or tail-to-tail regioregularities, all the aromatic protons of the unsubstituted benzene ring are in close contact with the different protons of the alanine residue of $n-1$ and $n+1$ m.r.u. (Figure 3a). This fact is due to the alternating distribution of alanine residues and aromatic rings on the helix ridges. On the contrary, in the case of a head-to-tail regioregularity, the unsubstituted and the substituted aromatic rings are located in the opposite helix ridges (Figure 3a). As a result, the proton at the *para* position of the unsubstituted benzene ring should afford a long-distance NOE cross peak with some alanine protons in a head-to-head or tail-to-tail sequence, whereas this NOE should not be observed in the case of a head-to-tail sequence. Therefore, the absence of this cross peak in the NOESY spectrum corroborates the head-to-tail regioregularity during the polymerization of poly-**1** (Figure 3c).

Interestingly, the head-to-tail structure observed for poly-(*S*)-**2** resembles the packing observed for a diphenylacetylene derivatized with an alanine methyl ester group [m-(*S*)-**2**] by X-ray diffraction[102] (Figure 3b).

Next, ECD studies were carried out for poly-(*S*)-**2** in DMF. As expected, no ECD signal was obtained until the sample was annealed at 80 °C for 4 hours. After annealing, an ECD trace with a first positive Cotton effect at 400 nm was obtained (Figure 4b). The dissymmetry factor (g_{abs}) obtained for poly-(*S*)-**2** was 1.8×10^{-3}, within the same range as the values reported for symmetric PDPAs or PPAs,[10,12,79] fact that corroborates both good stereo and regioregularities within poly-(*S*)-**2** with a screw sense excess.

To obtain more structural information, and to refine the helix adopted by poly-(*S*)-**2**, a 2D-crystal of this polymer was prepared using the protocol described by Yashima et al., which consists of spin coating a dilute DMF solution of poly-(*S*)-**2** on highly oriented pyrolytic graphite (HOPG) followed by annealing under the corresponding solvent atmosphere.[59] In our case, before spin coating the sample, the polymer was annealed in DMF at 80 °C for 4 h to induce a screw sense excess in the polyene backbone. High-resolution AFM images of poly-(*S*)-**2** reveal the presence of 2D crystals where single PDPA chains are packed in a parallel manner, one after the other, to form a right-handed (clockwise) pendant disposition with the periodic oblique stripes in 50° angles and a helical pitch of 6.35 nm (Figure 4a).

By combining the information obtained from the ECD and AFM studies of poly-(*S*)-**2** in DMF, we can state that the first positive Cotton band ($CD_{400}>0$) corresponds to a *P* helical structure described by the pendant groups (external helix). As with PPAs, PDPAs are made up of two coaxial

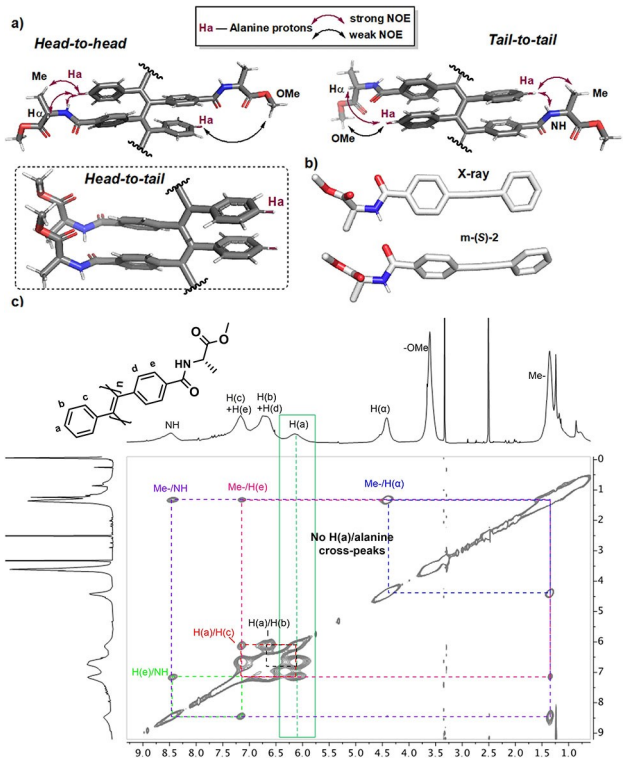

Figure 3. a) Dimeric model structures for a head-to-head, tail-to-tail and head-to-tail regioregularities of poly-(*S*)-**2**, emphasizing the expected NOE cross peaks for Ha. b) X-ray structure of m-(*S*)-**2**. c) NOESY spectrum of poly-(*S*)-2 in DMSO.

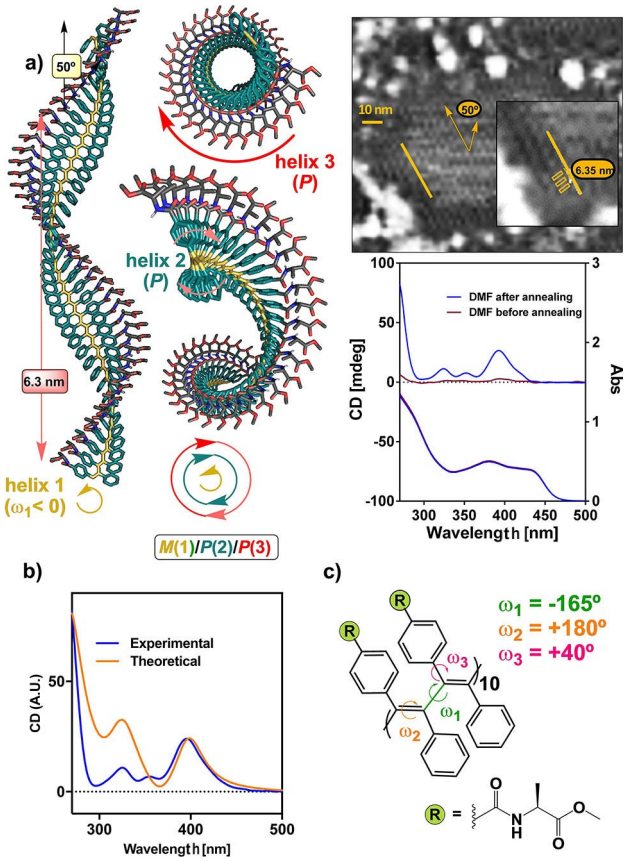

Figure 4. a) 3D structure of poly-(*S*)-**2**, AFM image of poly-(*S*)-**2** after annealing in DMF and CD/UV spectra of poly-(*S*)-**2** before and after annealing, $c = 0.5\ mg\,mL^{-1}$. b) Comparison between the experimental and theoretical ECD spectrum obtained for poly-(*S*)-**2**. c) Dihedral angles for the 12-mer oligomer used to compute the theoretical spectra.

helices, one described by the polyene backbone and the other described by the pendants.[70]

In order to stablish a relationship between internal and external helices, computational studies [TD-DFT(CAM–B3LYP)/3-21G][103–106] were performed on a *P* helix ($n = 20$ m.r.u.) for a PDPA with *trans-transoidal* skeleton, $\omega_1 = -165°$, $\omega_2 = 180°$, $\omega_3 = 40°$ (Figure 4a, d). In this model, the chiral substituents were removed to reduce the computational demands. The simulated ECD spectrum (Figure 4c and Supporting Information for detailed information) is in good agreement with the experimental one, which indicates that the proposed model is a good approximation to the structure of poly-(*S*)-**2**.

The helical structure described by an asymmetric PDPA in a *trans-transoidal* configuration is very different from the *cis-transoidal* helix described by a PPA. In a PDPA helix, three different helices coexist: a) helix 1, which is the classical internal helix described by the orientation between conjugated double bonds ($\omega_1 = -165°$) and which in this example (i.e., poly-(*S*)-**2**) is *M* oriented due to the negative value of ω_1 (Figures 4a, d); b) helix 2, which is the helix described between consecutive poly(diphenylacetylene) groups, and which rotates in the opposite direction to that defined by the dihedral angle between conjugated double bonds, helix 1 = ω_1 (so, in poly-(*S*)-**2**, is *P*; Figure 4a); and c) helix 3, which is present in PDPAs but does not exist in PPAs. This helix appears when the polyene backbone grows because of the *trans-transoidal* configuration of the polyene, resulting in a twist of the whole scaffold. The helical sense described by helix 3 is coincident with that described by helix 2, in this case a *P* helix (Figure 4a).

When analyzing the data obtained from the theoretical calculations, we could observe that unlike the PPAs, the PDPAs show a first Cotton band given by a combination of the poly(diphenylacetylene) backbone and not only by the polyene (see Supporting Information). Therefore, these results indicate that the correlation between the ECD signal and the helical sense of the polyene (ω_1) found in *cis*-PPAs cannot be applied to asymmetric PDPAs. In the latter it is found that, although the double bonds are *M* oriented (helix 1 $\omega_1 < 0$), the *P* orientation of consecutive diphenylacetylene m.r.u. (helix 2) in combination with the *P* orientation of the whole scaffold (helix 3), results in a final positive Cotton band. Thus, at this point we can state that in an asymmetric PDPA with a *trans-transoidal* helix, a first positive Cotton band at 400 nm indicates a helical structure with a *M*/*P*/*P* (helix 1/helix 2/helix 3) orientation. On the contrary, if the asymmetric PDPA shows a $CD_{400} < 0$, then the polymer adopts a *P*/*M*/*M* (helix 1/helix 2/helix 3) orientation.

Another interesting structural feature observed in PDPAs is found when the ECD and the UV spectra obtained for a DMF solution of poly-(*S*)-**2** are compared (Figure 4b). By looking at the two spectra, we can see that there is a mismatch between the first Cotton band in the ECD spectrum (400 nm) and the highest wavelength UV band (450 nm), corresponding the ECD Cotton band to the second band of the UV-spectrum (400 nm). To determine and characterize the electronic transitions responsible for these two UV-bands, theoretical ECD and UV studies were carried out for an $n = 12$ oligomer. The theoretical UV-spectrum reproduced the experimental one, showing two maxima at ca. 400 and 450 nm, being the first transition the one that produces the first Cotton band.

By analyzing the electron density differences involved in the transitions responsible of these bands, it was found that while the UV band at higher wavelengths, the one that is not ECD active, has an asymmetric contribution of the polyene and the aryl rings (Figure 5), the second UV band that corresponds to the first Cotton in the ECD spectrum shows a more symmetric contribution of each diphenylacetylene m.r.u. (Figure 5). These studies show how the UV and ECD Cotton bands appearing at ca. 400 and 450 nm are affected by the orientation of the diphenylacetylene m.r.u. and not just because of the polyene.

Interestingly, Kwak and co-workers found that a new ECD active signal could appear in the spectra of an asymmetric PDPA when measured in film or aggregated state. This band appears at ca. 450 nm, has the same sign as the Cotton band at 400 nm and was associated to a longitudinal coupling between polyene chains.[88,89]

Thus, we explored different solvents to try to study this ECD band further, choosing those where poly-(*S*)-**2** shows

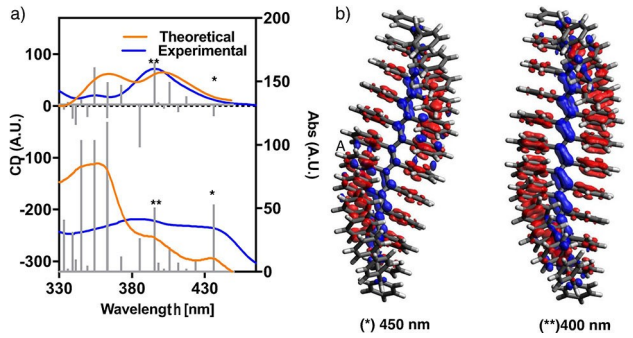

Figure 5. a) Comparison of calculated and experimental ECD and UV/Vis spectra of a 12-mer oligomeric PDPA model. b) Electron density differences of transitions responsible of UV and ECD bands at 400 and 450 nm.

poor solubility and appears as a dispersed aggregate. Of the different poly-(*S*)-**2** (0.5 mg mL^{-1}) solutions tested, only the MeCN solution was found to produce an ECD signal at 450 nm after annealing at 80 °C for 4 h.

In this solvent, the PDPA shows a negative Cotton band at 400 nm indicative of a *P*/*M*/*M* (helix 1/helix 2/helix 3) helical scaffold. Interestingly, AFM studies of poly-(*S*)-**2**, prepared in MeCN, showed the presence of superhelices that have a helical pitch of 14 nm and a width of 8 nm, parameters that correspond to a bundle of PDPA helices (Figures 6a–c).

Additionally, controlled nanoprecipitation[107,108] studies of poly-(*S*)-**2** in a THF/H_2O 1/1 v/v ratio were carried out to generate nanospheres that can produce this new ECD band at 450 nm due to the aggregation of poly-(*S*)-**2**. As expected, ECD studies of these nanospheres dispersed in THF/H_2O (Figure 6d–f) show again the presence of this new ECD band, which therefore can be attributed to an interaction between different PDPA chains, and more precisely, to a longitudinal coupling between asymmetric contributions of the polyene and the aryl rings as extracted from computational studies (Figure 5).

Dynamic Behavior of Asymmetric PDPAs

Once the helical structure of an asymmetric PDPA (i.e., poly-(*S*)-**2**) was puzzled out by the different structural techniques, the stimuli-responsive properties of poly-(*S*)-**2**, and therefore its dynamic behavior, were studied. In this case, the variation of the helical structures with solvents was analyzed after annealing at 80 °C for 4 h (Figure 7a). Interestingly, it is possible to observe the dynamic behavior of a chiral and asymmetric PDPA. This dynamic behavior was found before in achiral PDPAs bearing a *para*-benzoic group and where the sense can be enhanced towards *P* or *M* senses by interaction with the two enantiomers of a chiral amine.[79]

VCD studies were carried out to demonstrate that the helix inversion is associated to a conformational change at the pendant group. So, VCD spectra of poly-(*S*)-**2** in both $CDCl_3$ and DMSO-d_6 show activity in the carbonyl finger-

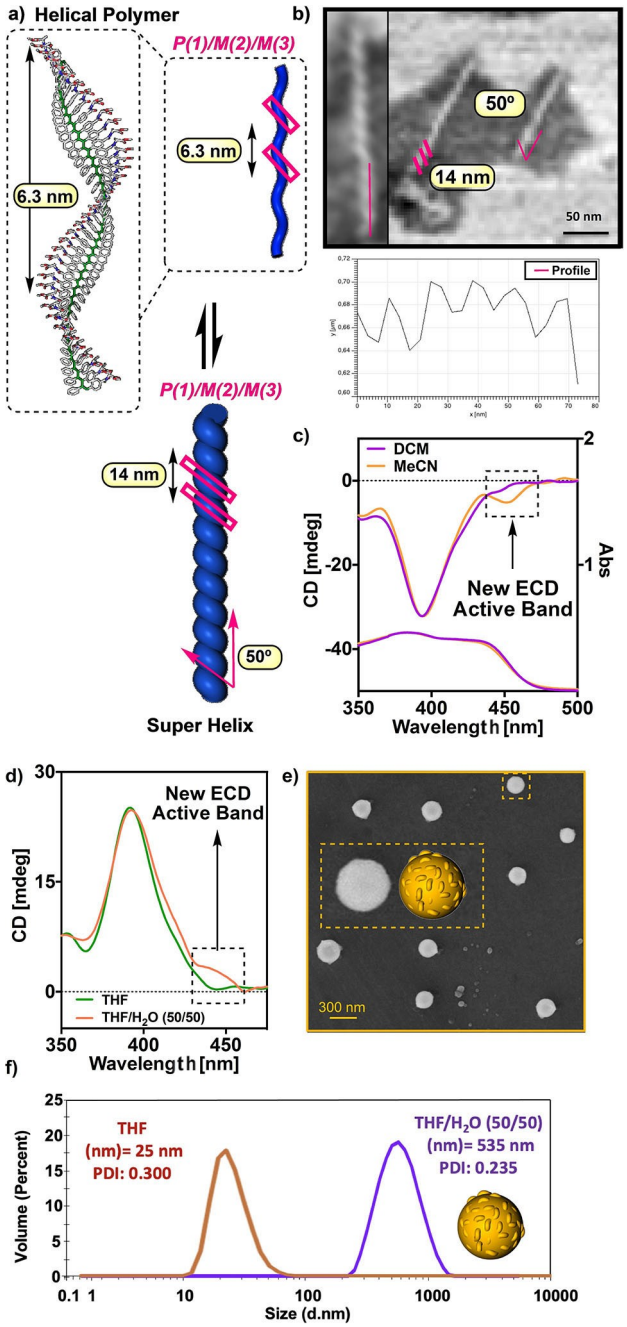

Figure 6. a) Conceptual representation of the superhelix formation. b) AFM image and height profile of the superhelical assemblies generated by poly-(*S*)-**2** during its annealing in MeCN. c) Comparison of the ECD spectra of poly-(*S*)-**2** in DCM (good solvent, non-aggregated state) and after annealing in MeCN (bad solvent, aggregated state) displaying the new low-energy ECD active band due to the formation of supramolecular aggregates. d) Comparison of the ECD spectra of poly-(*S*)-**2** in THF (good solvent, non-aggregated state) and THF/H_2O (1/1) (nanoprecipitated state) displaying the new low-energy ECD active band due to the formation of nanospheres. e) SEM image of the nanospheres generated by nanoprecipitation. f) DLS traces monitoring the nanoprecipitation process.

print region (Figure 7d). More precisely, the C=O stretching bands of the amide and the ester groups, 1650 and

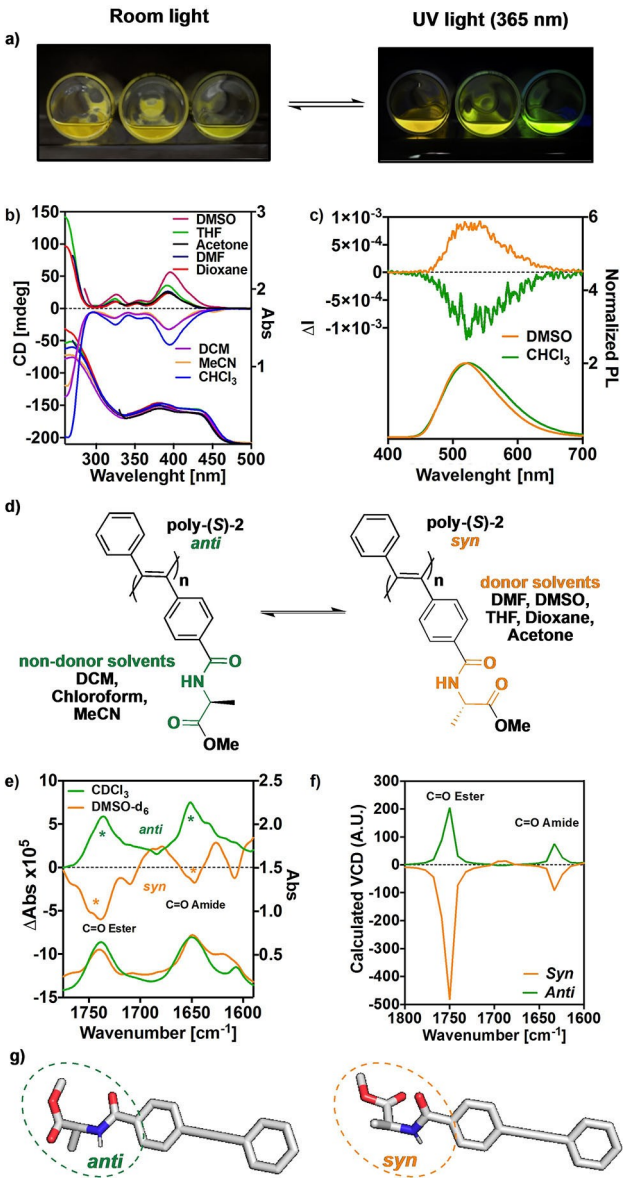

Figure 7. a) Photographs of poly-**1** and poly-(*S*)-**2** under room light and UV-light. b) ECD and UV spectra of poly-(*S*)-**2** in different solvents (0.5 mg mL^{-1}, 1 mm path). c) CPL spectra of poly-(*S*)-**2** (λ_{Exc} = 365 nm, 0.3 mg mL^{-1}). d) Schematic illustration of the solvent-triggered conformational change in the pendant group that promotes helix inversion. e) Experimental VCD spectra of poly-(*S*)-**2** in $CDCl_3$ and DMSO-d_6. f) Calculated VCD spectra of the monomeric units with *anti* and *syn* conformations. g) Optimized structures of the monomeric DPA units with *anti* and *syn* conformations employed to obtain the theoretical spectra depicted in (f).

1750 cm^{-1}, respectively, show positive bands in $CDCl_3$ [ECD-, *P*/*M*/*M* (helix 1/helix 2/helix 3)] and negative ones in DMSO-d_6 [ECD+, *M*/*P*/*P* (helix 1/helix 2/helix 3)] which are ascribed to *anti* and *syn* conformations at the pendant group respectively, as inferred from VCD theoretical calculations of the monomeric unit in both conformations (Figures 7c, f).

One of the most interesting features of PDPAs is that after adopting a screw sense excess, they result in circular polarized luminescent (CPL) active materials.[109,110] This unique property has found many applications in different cutting-edge fields such as security encoding[111] or CP-OLEDs among many others.[112] Consequently, CPL studies were carried out for poly-(*S*)-**2** in *P*, *rac* and *M* helical states exhibiting *P*, null and *M* CPL activity respectively (Figure 7b). The CPL sign is, as expected, coincident with that of the high energy band in the ECD spectra, indicating that a CPL (+) is due to a *M*/*P*/*P* (helix 1/helix 2/helix 3) arrangement, while a CPL (−) is ascribed to a *P*/*M*/*M* (helix 1/helix 2/helix 3) helical orientation.

Moreover, recently experimental, and computational CPL studies support the *trans-transoidal* structure for PDPAs.[113] The poor conformational flexibility in the polyene of PDPAs creates a reversing in the excited energy levels that permit an electronically dipole-allowed transition resulting in emissive materials, such as is observed here in poly-(*S*)-**2**. However, in the case of PPAs the emissive form of the helical scaffold is when the polyene backbone adopts just a *cis-cisoidal* configuration.[113]

The CPL emission was gauged by the dissymmetric factor defined as $|g_{lum}| = 2(I_L - I_R)/(I_L + I_R)$, being I_L and I_R the left- and right-handed luminescent emissions respectively. In both cases a maximum g_{lum} value of ca. $+/-1\times10^{-3}$ at 520 nm was obtained, with quantum yield values of $\varphi = 26$ and of $\varphi = 44$ for the $CHCl_3$ and DMSO solutions respectively. To the best of our knowledge, this system represents one of the few examples where the CPL sign can be switched,[114] paving the way to the design of new stimuli-responsive CPL active materials with enhanced properties and applications.

Conclusion

In summary, the combination of data collected from different structural techniques allowed us to build an approximated structure for an asymmetric PDPA prepared by polymerization with WCl_6/Ph_4Sn of a diphenyl acetylene monomer substituted with an active pentafluorophenyl ester (PFP) group. This polymer was further transformed into a chiral polymer by a post-functionalization reaction that incorporates L-alanine methyl ester into the pendants. To elucidate the secondary structure of the polymer, Raman and IR spectroscopies were used to discern between *Z* and *E* configurations of the double bonds. In this case, the polymer adopts mainly a *trans* configuration of the double bonds. 1D and 2D NMR experiments helped us to elucidate the regioregularity of the polymer, indicating a preferred head-to-tail polymerization reaction. AFM studies provided useful information related to different helical structural parameters such as helical pitch, packing angle and the orientation of the external helix described by the pendant groups. The use of molecular modelling, together with the constrains provided by the results of IR, Raman, NMR and AFM studies allowed us to build an approximate secondary structure for this polymer. Thus, poly-(*S*)-**2** adopts a preferred *trans-transoidal* helical scaffold that is formed by three different helices. Helix 1, described by the orientation

between conjugated double bonds; helix 2, described by the pendant groups; and helix 3, described by a twisting degree of the whole polymer chain and observed when the polymer grows. Computational studies on the model compound result in a theoretical ECD spectrum that resembles the experimental one and that allows us to demonstrate that in an asymmetric PDPA, the sign of the first Cotton band is ruled by helices 2 and 3, and not just by the orientation of the polyene backbone. Moreover, the present study also made it possible to explain why in different aggregation states, such as superhelices or nanospheres, a new ECD band appears because of a longitudinal coupling between polymer chains. Additionally, this work reveals the dynamic behavior of poly-(*S*)-**2** and shows how *P* or *M* helical senses can be induced by conformational changes at the pendant groups using external stimuli such as solvent donor ability, fact corroborated by a combination of VCD experiments and theoretical calculations. Finally, associated to this dynamic helical behavior, a dynamic circular polarized luminescence switch with a $|g_{lum}| = +/-1\times10^{-3}$ was obtained for poly-(*S*)-**2**, where a CPL (+) is produced by a *M*/*P*/*P* (helix 1/helix 2/helix 3) arrangement generated in donor solvents, while a CPL (−) is ascribed to a *P*/*M*/*M* (helix 1/helix 2/helix 3) helical orientation produced when poly-(*S*)-**2** is annealed in non-donor solvents.

The elucidation of the three-dimensional structure of a PDPA opens a new horizon in the development of functional materials due to the possibility of establishing structure/function relationships that can result in an improvement of the functionality of the polymer through a directed tuning of its secondary structure.

Acknowledgements

We thank Servicio de Microscopía Electrónica (RIAIDT, USC). Financial support from AEI (PID2019-109733GB-I00), Ministerio de Ciencia e Innovación (PID2019-107307RB-100 and PID2020-117605GB-100). Xunta de Galicia (ED431C 2018/30, ED431C 2021/40, Centro Singular de Investigación de Galicia acreditación 2019–2022, ED431G 2019/03, Beca Leonardo a Investigadores y Creadores Culturales 2020 de la Fundación BBVA and the European Regional Development Fund (ERDF) and is gratefully acknowledged. J.J.T. thanks MICINN for a FPU contract. We acknowledge CESGA for computational time and we also thank Servicio de Nanotecnología y Análisis de Superficies (CACTI-CINBIO, UVigo).

Conflict of Interest

The authors declare no conflict of interest.

Data Availability Statement

The data that support the findings of this study are available in the Supporting Information of this article.

Keywords: AFM images · Circular Polarized Luminescence Switch · Poly(diphenylacetylene)s · Secondary Structure · trans-transoid

[1] Y. Shen, C. F. Chen, *Chem. Rev.* **2012**, *112*, 1463–1535.
[2] T. Mori, *Chem. Rev.* **2021**, *121*, 2373–2412.
[3] E. S. Gauthier, R. Rodríguez, J. Crassous, *Angew. Chem. Int. Ed.* **2020**, *59*, 22840–22856; *Angew. Chem.* **2020**, *132*, 23036–23052.
[4] K. L. George, W. S. Horne, *Acc. Chem. Res.* **2018**, *51*, 1220–1228.
[5] Y. Ferrand, I. Huc, *Acc. Chem. Res.* **2018**, *51*, 970–977.
[6] E. A. John, C. J. Massena, O. B. Berryman, *Chem. Rev.* **2020**, *120*, 2759–2782.
[7] Y. Dorca, E. E. Greciano, J. S. Valera, R. Gomez, L. Sanchez, *Chem. Eur. J.* **2019**, *25*, 5848–5864.
[8] B. Adelizzi, N. J. Van Zee, L. N. de Windt, A. R. A. Palmans, E. W. Meijer, *J. Am. Chem. Soc.* **2019**, *141*, 6110–6121.
[9] P. Xing, Y. Zhao, *Acc. Chem. Res.* **2018**, *51*, 2324–2334.
[10] E. Yashima, K. Maeda, H. Lida, Y. Furusho, K. Nagai, *Chem. Rev.* **2009**, *109*, 6102–62111.
[11] M. Milton, R. Deng, A. Mann, C. Wang, D. Tang, M. Weck, *Acc. Chem. Res.* **2021**, *54*, 2397–2408.
[12] E. Yashima, N. Ousaka, D. Taura, K. Shimomura, T. Ijai, K. Maeda, *Chem. Rev.* **2016**, *116*, 13752–13990.
[13] J. G. Rudick, V. Percec, *Acc. Chem. Res.* **2008**, *41*, 1641–1652.
[14] E. Yashima, K. Maeda, Y. Furusho, *Acc. Chem. Res.* **2008**, *41*, 1166–1180.
[15] N. Liu, L. Zhou, Z. Q. Wu, *Acc. Chem. Res.* **2021**, *54*, 3953–3967.
[16] L. Zhou, X. H. Xu, Z. Q. Jiang, L. Xu, B. F. Chu, N. Liu, Z. Q. Wu, *Angew. Chem. Int. Ed.* **2021**, *60*, 806–812; *Angew. Chem.* **2021**, *133*, 819–825.
[17] J. H. Chu, X. H. Xu, S. M. Kang, N. Liu, Z. Q. Wu, *J. Am. Chem. Soc.* **2018**, *140*, 17773–17781.
[18] T. Yamamoto, R. Murakami, S. Komatsu, M. Suginome, *J. Am. Chem. Soc.* **2018**, *140*, 3867–3870.
[19] M. Núñez-Martínez, S. Arias, E. Quiñoá, R. Riguera, F. Freire, *Chem. Mater.* **2021**, *33*, 4805–4812.
[20] C. Zhao, S. Sun, W. L. Tong, M. C. W. Chan, *Macromolecules* **2017**, *50*, 6896–6902.
[21] R. Rodríguez, E. Suarez-Picado, E. Quiñoá, R. Riguera, F. Freire, *Angew. Chem. Int. Ed.* **2020**, *59*, 8616–8622; *Angew. Chem.* **2020**, *132*, 8694–8700.
[22] M. Alzubi, S. Arias, R. Rodríguez, E. Quiñoá, R. Riguera, F. Freire, *Angew. Chem. Int. Ed.* **2020**, *59*, 13365–13369.
[23] E. Suárez-Picado, E. Quiñoá, R. Riguera, F. Freire, *Angew. Chem. Int. Ed.* **2020**, *59*, 4537–4543; *Angew. Chem.* **2020**, *132*, 4567–4573.
[24] R. Ishidate, A. J. Markvoort, K. Maeda, E. Yashima, *J. Am. Chem. Soc.* **2019**, *141*, 7605–7614.
[25] K. Maeda, H. Hirose, N. Okoshi, K. Shimomura, Y. Wada, T. Ikai, S. Kanoh, E. Yashima, *J. Am. Chem. Soc.* **2018**, *140*, 3270–3276.
[26] R. Sakai, E. B. Barasa, N. Sakai, S. I. Sato, T. Satoh, T. Kakuchi, *Macromolecules* **2012**, *45*, 8221–8227.
[27] E. Yashima, K. Maeda, *Macromolecules* **2008**, *41*, 3–12.
[28] K. Maeda, E. Yashima, *Top. Curr. Chem.* **2006**, *265*, 47–88.
[29] R. Nonokawa, E. Yashima, *J. Am. Chem. Soc.* **2003**, *125*, 1278–1283.
[30] E. Yashima, K. Maeda, Y. Okamoto, *Nature* **1999**, *399*, 449–451.
[31] E. Yashima, K. Maeda, T. Matsushima, Y. Okamoto, *Chirality* **1997**, *9*, 593–600.
[32] M. Ando, R. Ishidate, T. Ikai, K. Maeda, E. Yashima, *J. Polym. Sci. Part A* **2019**, *57*, 2481–2490.

[33] C. Zhang, Y. Qiu, S. Bo, F. Wang, Y. Wang, L. Liu, Y. Zhou, H. Niu, H. Dong, T. Satoh, *J. Polym. Sci. Part A* **2019**, *57*, 1024–1031.
[34] R. P. Megens, G. Roelfes, *Chem. Eur. J.* **2011**, *17*, 8514–8523.
[35] S. Ikeda, R. Takeda, T. Fujie, N. Ariki, Y. Nagata, M. Suginome, *Chem. Sci.* **2021**, *12*, 8811–8816.
[36] Y. Nagata, R. Takeda, M. Suginome, *ACS Cent. Sci.* **2019**, *5*, 1235–1240.
[37] E. Anger, H. Iida, T. Yamaguchi, K. Hayashi, D. Kumano, J. Crassous, N. Vanthuyne, C. Roussel, E. Yashima, *Polym. Chem.* **2014**, *5*, 4909–4914.
[38] R. Ishidate, T. Sato, T. Ikai, S. Kanoh, E. Yashima, K. Maeda, *Polym. Chem.* **2019**, *10*, 6260–6268.
[39] D. Hirose, A. Isobe, E. Quiñoá, F. Freire, K. Maeda, *J. Am. Chem. Soc.* **2019**, *141*, 8592–8598.
[40] J. Shen, Y. Okamoto, *Chem. Rev.* **2016**, *116*, 1094–1138.
[41] K. Shimomura, T. Ikai, S. Kanoh, E. Yashima, K. Maeda, *Nat. Chem.* **2014**, *6*, 429–434.
[42] C. I. Simionescu, V. Percec, *Prog. Polym. Sci.* **1982**, *8*, 133–214.
[43] K. Morino, K. Maeda, Y. Okamoto, E. Yashima, T. Sato, *Chem. Eur. J.* **2002**, *8*, 5112–5120.
[44] J. G. Rudick, V. Percec, *Macromol. Chem. Phys.* **2008**, *209*, 1759–1768.
[45] M. Asahi, Y. Mawatari, R. Motoshige, Y. Yoshida, M. Tabata, *J. Polym. Sci. Part A* **2013**, *51*, 5177–5183.
[46] X. Q. Liu, J. Wang, Sh. Yang, E. Q. Chen, *ACS Macro Lett.* **2014**, *3*, 834–838.
[47] V. Percec, E. Aqad, M. Peterca, J. G. Rudick, L. Lemon, J. C. Ronda, B. B. De, P. A. Heiney, E. W. Meijer, *J. Am. Chem. Soc.* **2006**, *128*, 16365–16732.
[48] V. Percec, J. G. Rudick, M. Peterca, E. Aqad, M. R. Imam, P. A. Heiney, *J. Polym. Sci. Part A* **2007**, *45*, 4974–4987.
[49] V. Percec, M. Peterca, J. G. Rudick, E. Aqad, M. R. Imam, P. A. Heiney, *Chem. Eur. J.* **2007**, *13*, 9572–9581.
[50] V. Percec, J. G. Rudick, M. Peterca, P. A. Heiney, *J. Am. Chem. Soc.* **2008**, *130*, 7503–7508.
[51] A. Miyasaka, T. Sone, Y. Mawatari, S. Setayesh, K. Müllen, M. Tabata, *Macromol. Chem. Phys.* **2006**, *207*, 1938–1944.
[52] T. Ito, H. Shirakawa, S. Ikeda, *J. Polym. Sci. Polym. Chem. Ed.* **1974**, *12*, 11–20.
[53] Y. Yoshida, Y. Matawari, A. Motoshige, R. Motoshige, T. Hiraoki, M. Wagner, K. Müllen, M. Tabata, *J. Am. Chem. Soc.* **2013**, *135*, 4110–4116.
[54] R. Rodríguez, J. Ignés-Mullol, F. Sagués, E. Quiñoá, R. Riguera, F. Freire, *Nanoscale* **2016**, *8*, 3362–3367.
[55] J. Kumaki, *Polym. J.* **2016**, *48*, 3–14.
[56] J. Kumaki, S. I. Sakurai, E. Yashima, *Chem. Soc. Rev.* **2009**, *38*, 737–746.
[57] S. Sakurai, K. Okoshi, J. Kumaki, E. Yashima, *J. Am. Chem. Soc.* **2006**, *128*, 5650–5651.
[58] K. Okoshi, S. Sakurai, S. Ohsawa, J. Kumaki, E. Yashima, *Angew. Chem. Int. Ed.* **2006**, *45*, 8173–8176; *Angew. Chem.* **2006**, *118*, 8353–8356.
[59] S. I. Sakurai, K. Okoshi, J. Kumaki, E. Yashima, *Angew. Chem. Int. Ed.* **2006**, *45*, 1245–1248; *Angew. Chem.* **2006**, *118*, 1267–1270.
[60] V. Percec, J. G. Rudick, M. Peterca, S. R. Staley, M. Wagner, M. Obata, C. M. Mitchell, W. D. Cho, V. S. K. Balagurusamy, J. N. Lowe, M. Glodde, O. Weichold, K. J. Chung, N. Ghionni, S. N. Magonov, P. A. Heiney, *Chem. Eur. J.* **2006**, *12*, 5731–5746.
[61] F. Freire, E. Quiñoá, R. Riguera, *Chem. Commun.* **2017**, *53*, 481–492.
[62] I. Liu, T. Namikoshi, Y. Zang, T. Aoki, S. Hadano, Y. Abe, I. Wasuzu, T. Tsutsuba, M. Teraguchi, T. Kaneko, *J. Am. Chem. Soc.* **2013**, *135*, 602–605.
[63] H. Shirakawa, S. Ikeda, *Polym. J.* **1971**, *2*, 231–244.
[64] J. Tabei, M. Shiotsuki, F. Sanda, T. Masuda, *Macromolecules* **2005**, *38*, 9448.
[65] T. Kaneko, Y. Umeda, T. Yamamoto, M. Tereguchi, T. Aoki, *Macromolecules* **2005**, *38*, 9420–9426.
[66] B. Nieto-Ortega, R. Rodríguez, S. Medina, E. Quiñoá, R. Riguera, J. Casado, F. Freire, F. J. Ramírez, *J. Phys. Chem. Lett.* **2018**, *9*, 2266–2270.
[67] I. Palomo, R. Rodríguez, S. Medina, E. Quiñoá, J. Casado, F. Freire, F. J. Ramírez, *Angew. Chem. Int. Ed.* **2020**, *59*, 9080–9087; *Angew. Chem.* **2020**, *132*, 9165–9172.
[68] B. Fernández, R. Rodríguez, E. Quiñoá, R. Riguera, F. Freire, *ACS Omega* **2019**, *4*, 5233–5240.
[69] B. Fernández, R. Rodríguez, A. Rizzo, E. Quiñoá, R. Riguera, F. Freire, *Angew. Chem. Int. Ed.* **2018**, *57*, 3666–3670; *Angew. Chem.* **2018**, *130*, 3728–3732.
[70] F. Rey-Tarrío, R. Rodríguez, E. Quiñoá, R. Riguera, F. Freire, *Angew. Chem. Int. Ed.* **2021**, *60*, 8095–8103; *Angew. Chem.* **2021**, *133*, 8176–8184.
[71] M. Nozaki, D. Hirose, K. Maeda, *J. Chromatogr. A* **2020**, *1622*, 461173.
[72] Y. J. Jin, Y. G. Choi, G. Kwak, *Polymer* **2019**, *171*, 127–132.
[73] T. Sakaguchi, H. Shimada, T. Hashimoto, *Polym. Chem.* **2020**, *11*, 6471–6478.
[74] M. Miyairi, T. Taniguchi, T. Nishimura, K. Maeda, *Angew. Chem. Int. Ed.* **2020**, *59*, 14772–14780; *Angew. Chem.* **2020**, *132*, 14882–14890.
[75] X. Wang, H. Hu, W. Wang, A. Qin, J. Z. Sun, B. Z. Tang, *Polym. Chem.* **2015**, *6*, 7958–7963.
[76] X. Wan, Y. Gao, W. Wang, A. Qin, J. Z. Sun, B. Z. Tang, *Polym. Chem.* **2016**, *7*, 5312–5321.
[77] T. Aoki, Y. Kobayashi, T. Kaneko, E. Oikawa, Y. Yamamura, Y. Fujita, M. Teraguchi, R. Nomura, T. Masuda, *Macromolecules* **1999**, *32*, 79–85.
[78] H. Kim, D. Lee, S. Lee, N. Suzuki, M. Fujiki, C. L. Lee, G. Kwak, *Macromol. Rapid Commun.* **2013**, *34*, 1471–1479.
[79] K. Maeda, M. Nozaki, K. Hashimoto, K. Shimomura, D. Hirose, T. Nishimura, G. Watanabe, E. Yashima, *J. Am. Chem. Soc.* **2020**, *142*, 7668–7682.
[80] K. Maeda, D. Hirose, M. Nozaki, Y. Shimizu, T. Mori, K. Yamanaka, K. Ogino, T. Nishimura, T. Taniguchi, M. Moro, E. Yashima, *Sci. Adv.* **2021**, *7*, eabg5381.
[81] Y. Gao, X. Wang, J. Z. Sun, B. Z. Tang, *Chem. Rec.* **2015**, *15*, 524–532.
[82] K. U. Seo, Y. J. Jin, H. Kim, T. Sakaguchi, G. Kwak, *Macromolecules* **2018**, *51*, 34–41.
[83] W. Z. Yuan, A. Qin, J. W. Y. Lam, J. Z. Sun, Y. Dong, M. Häussler, J. Liu, H. P. Xu, Q. Zheng, B. Z. Tang, *Macromolecules* **2007**, *40*, 3159–3166.
[84] C. K. W. Jim, J. W. Y. Lam, C. W. T. Leung, A. Qin, F. Mahtab, B. Z. Tang, *Macromolecules* **2011**, *44*, 2427–2437.
[85] H. Kim, K. U. Seo, Y. J. Jin, C. L. Lee, M. Teraguchi, T. Kaneko, T. Aoki, G. Kwak, *ACS Macro Lett.* **2016**, *5*, 622–625.
[86] Y. J. Jin, K. U. Seo, Y. G. Choi, M. Teraguchi, T. Aoki, G. Kwak, *Macromolecules* **2017**, *50*, 6433–6438.
[87] H. Kim, Y. J. Jin, B. S. I. Kim, T. Aoki, G. Kwak, *Macromolecules* **2015**, *48*, 4754–4757.
[88] S. I. Kim, Y. J. Jin, W. E. Lee, R. Yu, S. J. Park, H. J. Kim, K. H. Song, G. Kwak, *Adv. Mater. Interfaces* **2014**, *1*, 1300029.
[89] D. Lee, H. Kim, N. Suzuki, M. Fujiki, C. L. Lee, W. E. Lee, G. Kwak, *Chem. Commun.* **2012**, *48*, 9275–9277.
[90] B. A. San Jose, S. Matsushita, K. Akagi, *J. Am. Chem. Soc.* **2012**, *134*, 19795–19807.
[91] K. Maeda, M. Maruta, K. Shimomura, T. Ikai, S. Kanoh, *Chem. Lett.* **2016**, *45*, 1063–1065.

[92] K. Maeda, M. Maruta, Y. Sakai, T. Ikai, S. Kanoh, *Molecules* **2016**, *21*, 1487–1500.
[93] K. A. Günay, P. Theato, H. A. Klok, *J. Polym. Sci. Part A* **2013**, *51*, 1–28.
[94] S. Leiras, E. Suarez-Picado, E. Quiñoá, R. Riguera, F. Freire, *Giant* **2021**, *7*, 100068.
[95] K. Cobos, R. Rodríguez, E. Quiñoá, R. Riguera, F. Freire, *Angew. Chem. Int. Ed.* **2020**, *59*, 23724–23730; *Angew. Chem.* **2020**, *132*, 23932–23938.
[96] Z. Fernández, B. Fernández, E. Quiñoá, R. Riguera, F. Freire, *Chem. Sci.* **2020**, *11*, 7182–7187.
[97] S. Arias, M. Núñez-Martínez, E. Quiñoá, R. Riguera, F. Freire, *Polym. Chem.* **2017**, *8*, 3740–3745.
[98] A. Takeda, T. Sakaguchi, T. Hashimoto, *Polymer* **2009**, *50*, 5031–5036.
[99] Y. J. Jin, H. Kim, D. Y. Hwang, M. Teraguchi, T. Kaneko, T. Aoki, G. Kwak, *Mol. Cryst. Liq. Cryst.* **2017**, *645*, 50–57.
[100] A. C. Pauly, P. Theato, *Polym. Chem.* **2012**, *3*, 1769–1782.
[101] C. I. Simionescu, V. Percec, S. Dumitrescu, *J. Polym. Sci. Polym. Chem. Ed.* **1977**, *15*, 2497–2509.
[102] Deposition Number 2130256 contains the supplementary crystallographic data for this paper. These data are provided free of charge by the joint Cambridge Crystallographic Data Centre and Fachinformationszentrum Karlsruhe Access Structures service.
[103] E. Runge, E. K. U. Gross, *Phys. Rev. Lett.* **1984**, *52*, 997–1000.
[104] Y. Yanai, D. P. Tew, C. C. A. Handy, *Chem. Phys. Lett.* **2004**, *393*, 51–57.
[105] M. J. G. Peach, T. Helgaker, P. Salek, T. W. Keal, O. B. Lutnæs, D. J. Tozer, N. C. Handy, *Phys. Chem. Chem. Phys.* **2006**, *8*, 558–562.
[106] Gaussian 03 (Revision B-04), M. J. Frisch, G. W. Trucks, H. B. Schlegel, G. E. Scuseria, M. A. Robb, J. R. Cheeseman, J. A. Montgomery Jr., T. Vreven, K. N. Kudin, J. C. Burant, J. M. Millam, S. S. Iyengar, J. Tomasi, V. Barone, B. Mennucci, M. Cossi, G. Scalmani, N. Rega, G. A. Petersson, H. Nakatsuji, M. Hada, M. Ehara, K. Toyota, R. Fukuda, J. Hasegawa, M. Ishida, T. Nakajima, Y. Honda, O. Kitao, H. Nakai, M. Klene, X. Li, J. E. Knox, H. P. Hratchian, J. B. Cross, C. Adamo, J. Jaramillo, R. Gomperts, R. E. Stratmann, O. Yazyev, A. J. Austin, R. Cammi, C. Pomelli, J. W. Ochterski, P. Y. Ayala, K. Morokuma, G. A. Voth, P. Salvador, J. J. Dannenberg, V. G. Zakrzewski, S. Dapprich, A. D. Daniels, M. C. Strain, O. Farkas, D. K. Malick, A. D. Rabuck, K. Raghavachari, J. B. Foresman, J. V. Ortiz, Q. Cui, A. G. Baboul, S. Clifford, J. Cioslowski, B. B. Stefanov, G. Liu, A. Liashenko, P. Piskorz, I. Komaromi, R. L. Martin, D. J. Fox, T. Keith, M. A. Al-Laham, C. Y. Peng, A. Nanayakkara, M. Challacombe, P. M. W. Gill, B. Johnson, W. Chen, M. W. Wong, C. Gonzalez, J. A. Pople, Gaussian, Inc., Pittsburgh, PA, **2003**.
[107] H. Fessi, F. Puisieux, J. P. Devissaguet, N. Ammoury, S. Benita, *Int. J. Pharm.* **1989**, *55*, R1–R4.
[108] J. P. Rao, K. E. Geckeler, *Prog. Polym. Sci.* **2011**, *36*, 887–913.
[109] Y. Deng, M. Wang, Y. Zhuang, S. Liu, W. Huang, Q. Zhao, *Light: Sci. Appl.* **2021**, *10*, 1–18.
[110] H. Tanaka, Y. Inoue, T. Mori, *ChemPhotoChem* **2018**, *2*, 386–402.
[111] L. E. MacKenzie, R. Pal, *Nat. Chem. Rev.* **2021**, *5*, 109–124.
[112] K. Dhbaibi, L. Abella, S. Meunier-Della-Gatta, T. Roisnel, N. Vanthuyne, B. Jamoussi, G. Pieters, B. Racine, E. Quesnel, J. Autschbach, J. Crassous, L. Favereau, *Chem. Sci.* **2021**, *12*, 5522–5533.
[113] S. Wang, D. Hu, X. Guan, S. Cai, G. Shi, Z. Shuai, J. Zhang, Q. Peng, X. Wan, *Angew. Chem. Int. Ed.* **2021**, *60*, 21918–21926; *Angew. Chem.* **2021**, *133*, 22089–22097.
[114] Y. Gao, C. Ren, X. Lin, T. He, *Front. Chem.* **2020**, *8*, 1–17.

Manuscript received: November 6, 2021
Accepted manuscript online: January 13, 2022
Version of record online: January 24, 2022